Tutor/s

Dra. Dolors Velasco Castrillo
Departament de Química Inorgànica i Orgànica

Dr. Jaume Garcia Amorós
Departament de Química Inorgànica i Orgànica

Grau de Química

Treball Final de Grau

Synthesis and characterization of photoisomerizable azo-based organic compounds as a component of liquid crystal macromolecular systems.

Síntesi i caracterització d'azo compostos fotoisomeritzables orgànics com a components de sistemes cristall-líquid macromoleculars.

Raúl Artal López

January 2019

UNIVERSITAT DE BARCELONA

B:KC Barcelona Knowledge Campus
Campus d'Excel·lència Internacional

No pierdas el tiempo buscando un obstáculo, tal vez no haya ninguno.

Franz Kafka

Primerament, m'agradaria agrair als meus tutors, la Dra. Dolors Velasco així com el Dr. Jaume García per tot el temps que m'hi han dedicat, així com per endinsar-me en un mon completament desconegut com eren els elastòmers.

Voldria agrair també a tot el Grup 04 per haver-me fet sentir com a casa des del primer dia.

Als meus pares, per ser sempre exemple i referent per a mi, i per la seva incondicional confiança, sense vosaltres mai hagués pogut arribar fins aquí.

A l'Ernesto, el Guillem, el Pol i el Robert, per haver-me acompanyat al llarg dels anys en aquest viatge, les infinites jornades d'estudi no haguessin estat el mateix sense vosaltres.

A Kamila, por ser siempre el refugio al que puedo acudir, por tu apoyo sin medida, y por todas las sonrisas que sabes sacarme en mis momentos de panico, gracias.

REPORT

CONTENTS

1. SUMMARY 3
2. RESUM 5
3. INTRODUCTION 7
3.1. Liquid-crystalline materials 7
3.2. Photoactive liquid crystalline materials for actuation 9
3.3. Our system 10
4. OBJECTIVES 12
5. RESULTS AND DISCUSSION 13
5.1. Synthesis of the monomers 13
5.2. Characterisation of the monomers 18
5.2.1. Polarised optical microscopy (POM) 18
5.2.2. Thermal *cis*-to-*trans* isomerisation kinetics 19
5.3. Synthesis of the LSCEs 21
5.4. Characterisation of the LSCEs 22
5.4.1. Differential scanning calorimetry (DSC) 22
5.4.2. Swelling experiments 24
5.4.3. X-ray scattering 25
5.4.4. Polarised optical microscopy (POM) 28
6. EXPERIMENTAL SECTION 29
6.1. Materials and methods 29
6.1.1. Anhydrous solvents 29
6.1.2. Thin layer and flash column chromatography 29
6.1.3. Nuclear Magnetic Resonance spectroscopy (NMR) 29
6.1.4. Fourier transform infrared spectroscopy (FT-IR) 29
6.1.5. Analytical Weights 29
6.1.6. UV-Vis spectroscopy 29

6.1.7. Kinetic experiments 30
6.1.8. X-Ray diffraction experiments (XRD) 30
6.1.9. Swelling experiments 30
6.1.10. Polarised optical microscopy (POM) 30
6.1.11. Differential scanning calorimetry (DSC) 30
6.1.12. Spin-casting technique 31
6.2. Synthesis of the monomers 31
6.2.1. 1,4-Bis(10-undecenyloxy)benzene (**1**) 31
6.2.2. 4-hydroxy-4'-methoxyazobenzene (**2**) 31
6.2.3. 4-(5-hexenyloxy)-4'-methoxyazobenzene (**3**) 32
6.2.4. 4-(methoxy)-4'-(10-undecenyloxy)azobenzene (**4**) 32
6.2.5. undecenyloxybenzene (**5**) 33
6.3. Synthesis of the liquid single crystal elastomers 33
7. CONCLUSIONS 35
8. REFERENCES AND NOTES 37
9. ABBREVIATIONS, ACRONYMS AND SYMBOLS 39
APPENDIX 1: SCHEMATIC PHASE DIAGRAM FOR AZOCOMPOUND 4 43
APPENDIX 2: DSC THERMOGRAMS OF THE ELASTOMERS 44
APPENDIX 3: XRD DIFFRACTOGRAMS FOR THE ELASTOMERS 47

1. SUMMARY

Smart materials are having a great deal of attention due to their endless applications in a wide range of technological areas as artificial actuation. Specifically, photoactive materials are very attractive since light, the energy source needed for their triggering, is environmentally friendly, free and cheap. Azobenzene derivatives are the chromophores of common choice for the design of light-sensitive materials due to their reversible isomerisation. Indeed, the introduction of these particular organic chromophores into liquid-crystalline polymers enables the modulation of their macroscopic properties like, for instance, their dimensions and shape.

The first part of this project has involved the design and synthesis of two novel azobenzene derivatives. The structural identity of the azo compounds prepared has been confirmed by means of IR and ^{1}H NMR spectroscopies. Their mesomorphic and photochromic behaviour has been investigated by means of polarized optical microscopy and time-resolved UV-Vis spectroscopy.

The second part of the TFG implied the integration of these chromophores into liquid single crystal elastomers (LSCEs), *i.e.* weakly cross-linked polymer networks exhibiting a macroscopic orientation of the directors. As a whole, our LSCEs consist of a photoactive azobenzene-based monomer, a cross-linker and a mesogen. The introduction of an additional alkoxyphenyl comonomer has been considered in order to modulate the mesophase-to-isotropic phase transition temperature of the final material. Such feature is expected to pave the way to achieve photoactuating materials which can be operated under ambient conditions.

All LSCEs have been prepared via the spin casting technique in three steps developed by Finkelmann and collaborators and further characterised by means of several techniques such as polarised optical microscopy, swelling experiments, differential scanning calorimetry and x-ray diffraction.

Keywords: Azobenzene derivatives, *cis*-to-*trans* isomerisation, liquid-crystalline elastomers, organic synthesis, photoactuating materials, smart materials.

2. RESUM

Els materials intel·ligents estan essent àmpliament estudiats actualment degut a les seves múltiples aplicacions en àrees referents a la tecnologia com ara actuació artificial. Concretament, els materials foto-actius ja que requereixen d'una font d'energia renovable, respectuosa amb el medi ambient i barata com és la llum. Els cromòfors emprats habitualment son els derivats d'azobenzens degut a la seva isomerització reversible. La incorporació d'aquest tipus de cromòfors a sistemes cristall-líquid polimèrics permet la modulació de propietats macroscòpiques com ara bé, les seves dimensions i la seva forma.

La primera part d'aquest treball ha estat dedicada al disseny i la síntesi dels derivats d'azobenzens i la seva posterior determinació estructural. Aquesta ha estat determinada per mitjà de les tècniques comunes d'elucidació estructural com ara l'espectroscòpia IR i el RMN ^{1}H. Addicionalment, el seu comportament meromòrfic ha estat estudiat per mitjà de microscòpia òptica polaritzada així com els processos d'isomerització per mitjà de espectroscòpia UV-Vis.

Posteriorment, la introducció d'aquest azo compostos a un sistema elastòmer cristall-líquid monodomini, on tots els vectors directors estan macroscòpicament alineats, ha estat estudiada. Els sistemes escollits consisteixen en un monòmer derivat d'azobenzè, un agent cross-linker i un mesogen. Durant el transcurs del treball, s'ha considerat la introducció d'un alcoxifenil com a co-monomer per tal de variar la temperatura de transició entre la mesofase obtinguda i la fase isotròpica. Aquest fet, s'espera que pugui conduir cap a l'obtenció de sistemes foto-actius que puguin ser operats en condicions ambientals.

Tots els elastòmers han estat preparats seguint la tècnica d'spin càsting en tres etapes desenvolupada per el grup de recerca de en H. Finkelmann i posteriorment caracteritzats mitjançant microscòpia òptica polaritzada, calorimetria diferencial d'escombratge, experiments de swelling i difracció de raigs X.

Paraules clau: derivats d'azobenzens, isomerització *cis*-a-*trans*, elastòmers cristall-líquid, síntesi orgànica, materials foto-actius, materials intel·ligents.

3. INTRODUCTION

3.1. Liquid-crystalline materials

Liquid-crystalline materials, which have an intermediate structure between crystalline solids and isotropic liquids, are garnering a great deal of attention during the last decades since they open the door to new amazing applications that would be otherwise impossible to achieve with their conventional solid and liquid counterparts. Besides many others, liquid-crystalline materials find application in a wide variety of areas such as thermography, artificial actuation, cosmetics, enantioselective synthesis, shape memory materials and micro-robotics.[1,2,3,4] In addition, we also find this kind of materials in the most common electronic devices that we use on a daily basis, such as cell phones or TV.

Liquid crystals (LCs), which were discovered in 1899 by F. Reinitzer[5], uniquely combine the molecular order of the crystalline solids and the fluidity of the isotropic liquid state. This intermediate state of matter is named liquid-crystalline state or mesophase[6]. The mesophase is formed by molecules called mesogens and endow the final material with a liquid-crystalline behaviour. Although the degree of order present in a mesophase is lower than that found in traditional solids, it is high enough to induce a great anisotropy in the properties of the resulting system. In this way, liquid crystals are fluids with anisotropic properties because of the mesogens tendency to point to a common direction called director, ***n*** (Figure 1).

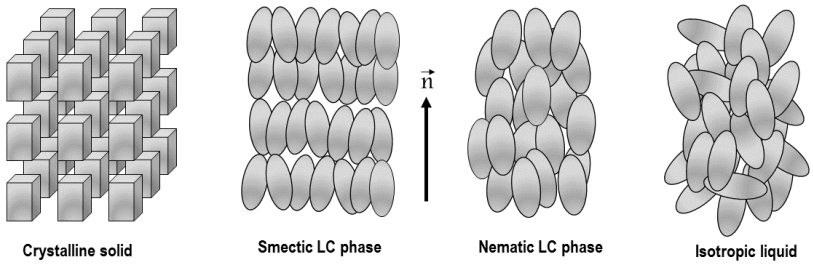

Figure 1. Molecular distribution within the solid, smectic and nematic liquid-crystalline and isotropic liquid state.

Liquid crystals are generally divided into two different groups: low molar mass LCs –discrete molecules with stable mesophases– and high molar mass LCs, *i.e*. macromolecular systems that show liquid-crystalline properties. In turn, high molar mass LCs can be either linear, named as linear liquid-crystalline polymers (LCPs), or cross-linked, named liquid-crystalline elastomers (LCEs). The basic difference between LCPs and LCEs is the presence of a cross-linking agent in the latter that endows the resulting material with its characteristic elastic properties.[7]

Both low and high molecular mass liquid crystals can be subdivided in two different categories according to the magnitude that controls the stability of the mesophase: thermotropics and lyotropics. Thermotropic LCs show different mesophases, which are stable only within a determined temperature range. On the other hand, the formation of a lyotropic mesophase depends mainly on the mesogen concentration and the solvent where it is dissolved but also slightly on the temperature. This work will be focused on thermotropic LCs.

According to geometrical features, thermotropic LCs can be divided into two different families: calamitics and discotics. Calamitic LCs present a rod-like geometry. In this case, the director is parallel to the longest axis of the mesogen. Otherwise, discotic LCs present a disk-like shape and the director is perpendicular to the plane of the molecule.

Thermotropic calamitic LCs show different mesophases depending on their intrinsic order: nematic, smectic and cholesteric (see Figure 1). In the nematic phase, which is the simplest of the liquid-crystalline phase, the molecules are oriented parallel to their longest axis. This particular phase shows long-range orientational order, but lacks of short-range positional order. Smectic phases exhibit both orientational and positional order. The cholesteric phase (or chiral nematic phase) is organized in nematic layers with the director rotating a determined angle from one layer to the next one. This work will be focused on the use of calamitic nematic LCs.

The macroscopic properties of liquid-crystalline materials can be easily changed by applying suitable external stimuli such as light, temperature, magnetic fields, changes of solvent or pH, etc. These external inputs alter the molecular and supramolecular organization of the system, which reflects in dramatic variations of its macroscopic properties. Specifically, nematic mesophase is the less ordered and less viscous among all the liquid-crystalline phases enabling a much easier modification of the mesogens alignment by applying suitable external stimuli. As a result, liquid crystals showing nematic mesophases are by far the ones having a greater impact in modern technology, and thus, the most commonly used for applications.

3.2. Photoactive liquid-crystalline materials for actuation

Light, a cheap, sustainable and clean energy source, allows a rapid and wireless control of the material properties. For photo actuation in LCs to take place, it is needed either intrinsically photoactive mesogens or provide the material with some photoactive molecules. Several photochromes are well known in organic chemistry to be suitable for this purpose, such as spiropyranes, spirooxazines, stilbenes, azobenzenes, fulgides and viologens, among others. There are two types of photochromes depending on the thermal stability of the photogenerated isomer:

- *T-type*, or thermally reversible, which return to their stable form with temperature (*e.g.* azobenzenes, stilbenes or spiropyranes).
- *P-type*, or photochemically reversible, which return to their stable isomer upon irradiation with light of the appropriate wavelength (*e.g.* diarylethenes or fulgides).

Azobenzenes are the most used photochromic group for designing light-controlled materials because of their reversible isomerisation process between their two isomers: *trans* and *cis* (Figure 2).[8] Indeed, azobenzenes interconvert both isomers with light of a particular wavelength: UV light, for the *trans*-to-*cis* conversion, and visible light, for the *cis*-to-*trans* isomerisation. In addition, the *cis* isomer is less stable than the *trans* one because of the steric hindrance.

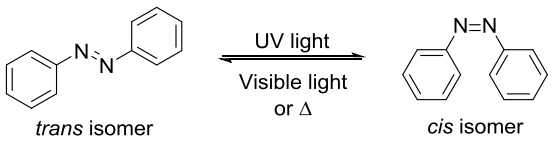

Figure 2. *trans*-to-*cis* isomerisation of an azobenzene.

When an azobenzene-containing liquid-crystalline material is irradiated with light of the appropriate wavelength, the bent *cis* form of the chromophore is generated, and all the LC molecules are disorganized. The system returns to the initial state when turning off the irradiation due to the recovery of the thermodynamically stable *trans* isomer.[9] Thus, the *cis* isomer acts as an impurity on the system, decreasing the degree of order, due to its bent form. If the azobenzene chromophore is covalently attached to a liquid-crystalline polymeric network, this phenomenon will result in a macroscopic contraction of the material.

Although both LCPs and LCEs have the characteristic molecular organization of LCs, it extends only along microscopic domains. Thus, in these multidomain systems, the director

changes abruptly from one domain to another. Consequently, the response of these materials to non-polarised light is not significant. Therefore, the use of polarised light is needed to obtain important photoactuation. Even having some limitations, as the one mentioned before, there are multidomain LCE systems with very good mechanical responses upon illumination.[10]

The use of non-polarised light is preferable since it simplifies enormously the operation of the material and expands its applicability. Hence, macroscopic orientation of the domains in one single direction is needed to maximize the response of these materials, known as liquid single crystal elastomers (LSCEs). Specifically, LSCEs are weakly cross-linked polymers with a macroscopic orientation of the director.

3.3. Our system

The desired elastomer is based in four components that will provide to it the desired properties such as the liquid-crystalline state, the photo actuation and the elastic behaviour. These four components are:

- A polysiloxane matrix, and more specifically, polymethylhydrosyloxane.
- The mesogen, that will provide our system a nematic liquid crystalline phase.
- The azobenzene derivative, which will induce the photoactuation of the elastomer due to its *cis*-to-*trans* isomerisation process (Figure 3).
- The isotropic cross-linker, that will give the elastic behaviour to the elastomers by bonding together two polysiloxane chains.

The macroscopic actuation of that elastomeric systems is closely related to the content of the azobenzene derivative in the elastomer. The macroscopic deformation, in this case, will be bigger as the amount of azobenzene increases. As it has been explained before, when azobenzene-containing compounds are isomerised by light, the rod-like geometry of the *trans* isomer is lost and the order present in the system decreases, due to the bent geometry of the *cis* isomer (Figure 2).

As it can be seen in Figure 3, the order parameter decreases abruptly when passing from the nematic phase (low temperatures) to the isotropic one (high temperatures). In addition, both isomers have different nematic-to-isotropic transition temperatures, so there ir a range of temperatures in which a high deformation can be induced to the elastomeric system by means of a photo-induced phase transition, causing a huge macroscopic response.

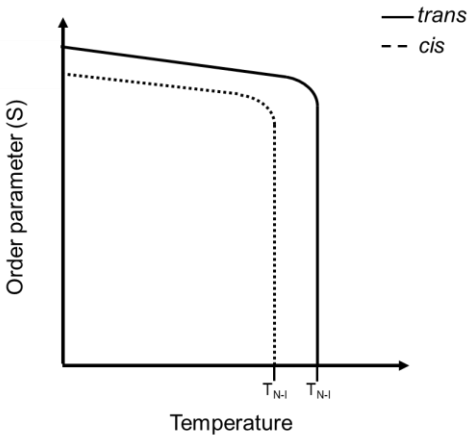

Figure 3. Schematic variation of the order parameter with temperature.

T_{N-I} values are generally well-above the room temperature. In this way, a high concentration of azobenzene chromophores is required in order to achieve efficient photoactuation under ambient conditions. In this line, a systematic study of the effect of the azobenzene concentration will be performed.

On the other hand, the introduction of additional monomers will be also considered in order to decrease that nematic-to-isotropic transition temperature to get systems that can be operated under ambient conditions.

4. OBJECTIVES

The main purpose of this project is the preparation of photoactive azo-based liquid-crystalline elastomers and its posterior characterisation.

The concrete objectives of this work are listed below:

- Design, synthesis and purification of photoactive azo-based derivatives.
- Characterisation of the synthetised monomers by means of standard structural characterisation techniques such as IR and ^{1}H NMR spectroscopies.
- Study of the isomerisation process of the azo-compounds by means of time-resolved UV-vis spectroscopy.
- Synthesis of photoactive azo-based liquid-crystalline elastomers.
- Study of the impact of the azo-based monomers content to the mesomorphic behaviour of the final material.
- Characterisation of the elastomers by means of X-ray diffraction, differential scanning calorimetry (DSC) and polarised optical microscopy and swelling experiments.

5. RESULTS AND DISCUSSION

5.1. SYNTHESIS OF THE MONOMERS

The target elastomeric system is based in four components: the cross-linker, which will provide the desired elastic behaviour, the mesogenic units, which will induce the long-range order at the nanoscale, the photoactive azo moieties, which will induce the deformation of the material upon illumination with light of the appropriate wavelength, and the polysiloxane, the commercially-available main polymeric backbone.

The cross-linking agent used will be 1,4-bis(10-undecenyloxy)benzene (**1**). The preparation of the isotropic cross-linker is shown in Figure 4.

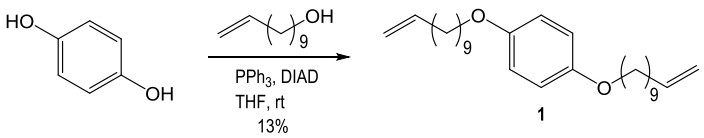

Figure 4. Synthesis of the cross-linker agent **1**.

1 was obtained via a Mitsunobu reaction between 1,4-benzoquinone and 10-undecen-1-ol. **1** could be also obtained by means of a Williamson reaction, but because of the relatively high price of the alkyl halide, the Mitsunobu reaction was considered as the most appropriate option. In this reaction a dehydrative coupling takes place between the phenol functions of 1,4-benzoquinone and 10-undecen-1-ol. Firstly, PPh_3 reacts with diisopropyl azodicarboxylate (DIAD) generating a phosphonium intermediate. A betaine intermediate is then formed from the reaction between the phenol function of 1,4-benzoquinone and DIAD, that activates that group to be alkylated.[11,12] 2 eq. of 10-undecen-1-ol were used. The reaction took place obtaining **1** in a yield of 13 %.

IR spectrum shows that the reaction was successfully achieved. The signal corresponding to the -OH stretching is no longer observable, and the appearance of the Csp^2-H stretching at 3080 cm^{-1} is observed. Also, the Csp^3-H stretching at 2933 cm^{-1} and the C=C stretching at 1642 cm^{-1}

were also detected. On the other hand, a ^{1}H NMR spectrum was recorded in $CDCl_3$ to evaluate the purity of the obtained product (Figure 5).

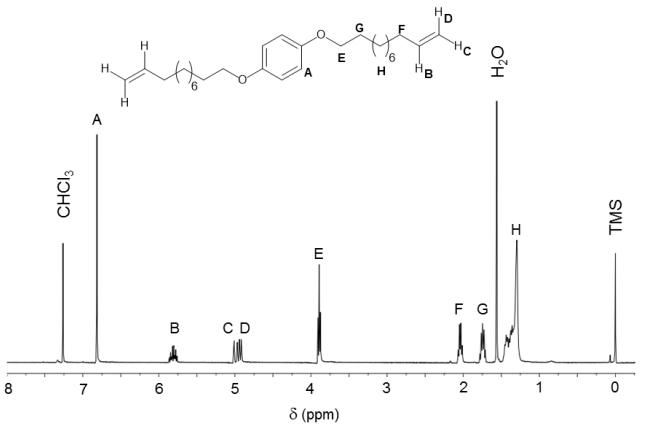

Figure 5. ^{1}H NMR spectrum of the cross-linker **1** in $CDCl_3$.

As it can be observed in the ^{1}H NMR just one signal integrating 4 protons is present for the aromatic protons, according to the *para* di-substitution of the benzene ring. A triplet which integrates 2 protons for the -O-C*H*$_2$-CH$_2$ is observed with a coupling constant of 6.5 Hz. Also, the appearance of two very similar multiplets near 5 ppm evidences the presence of the terminal double bond as a consequence of the different coupling constants for *cis* and *trans* protons. In addition, the signal for all the aliphatic protons as a multiplet between 1.47 and 1.23 ppm with an integral of 24 protons.

The mesogenic and photoactive units were synthetized from 4-methoxyaniline following the synthetic scheme shown in Figure 6**.**

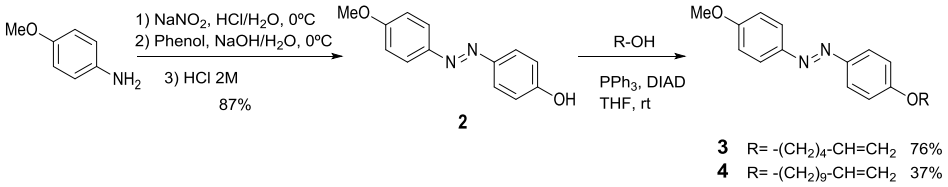

Figure 6. Synthetic route for obtaining azo derivatives **3** and **4**.

In the first step for synthetizing 4-hydroxy-4'-methoxyazobenzene (**2**), the $NaNO_2$ forms HNO_2 in presence of hydrochloric acid. When water is eliminated from protonated nitrous acid, the

nitrosonium ion is generated. That nitrosonium ion, which is an excellent electrophile, will react with aniline forming the diazonium ion. That diazonium ion is unstable at room temperature and in the presence of an activated benzene ring, in our case the phenoxide, can undergo an electrophilic aromatic substitution, obtaining **2** in a yield of 87%.

To determine if the corresponding azo compound was successfully prepared, an IR spectrum and also a ^{1}H NMR were recorded (Figure 7). In the IR spectrum, an OH st band appears at 3404 cm^{-1} that shows that the reaction has taken place correctly. In addition, C_{sp2}-H st and C_{sp3}-H st bands are present at 3026 cm^{-1} and 2950 cm^{-1}, respectively.

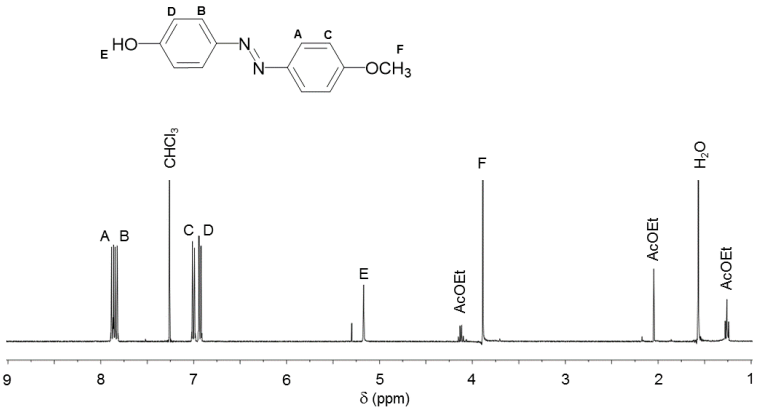

Figure 7. ^{1}H NMR spectrum for azo compound **2** in $CDCl_3$.

As it was expected, in the ^{1}H NMR spectrum appears 4 doublet signals for two aromatic protons each one, and two singlets corresponding for the O-H proton and also for the -OCH_3 with an integral of one and three protons respectively. Thus, the reaction was successfully achieved.

Azo compounds 4-(5-hexenyloxy)-4'-methoxyazobenzene (**3**) and 4-(methoxy)-4'-(10-undecenyloxy)azobenzene (**4**) were obtained via Mitsunobu reaction, where the PPh_3 combines with DIAD activating the alcohol group of compound **2** as a leaving group so the following alkylation will take place easily. In the IR spectra of both compounds it can be easily identified the disappearance of the -OH st signal, showing that alkylation has been achieved, and also, the appearance of the signal for the C_{sp3}-H st at 2985 and 2950 cm^{-1}. The ^{1}H NMR spectrum for compound **3** is shown below:

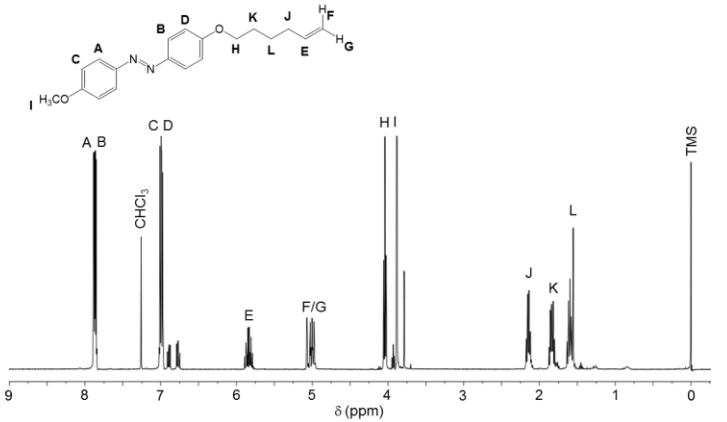

Figure 8. ^{1}H NMR spectrum for azo compound **3** in $CDCl_3$.

As it is shown in Figure 8, the appearance of 3 signals between 2.16 and 1.53 ppm points out that the alkylation reaction has been achieved. Also, the triplet at 4.04 ppm with a coupling constant of 6.4 Hz evidences the presence of the -O-CH_2-CH_2- fragment and the successful coupling between the lateral alkyl chain and the azobenzene core.

The ^{1}H NMR for the analogue azo-compound **4** is shown below:

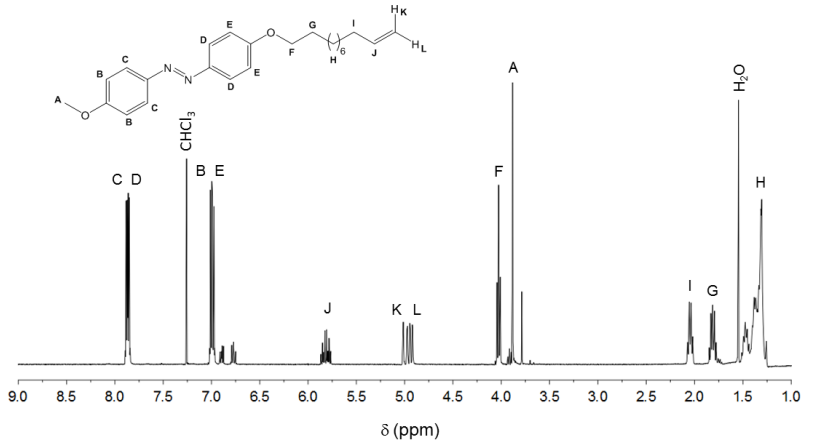

Figure 9. ^{1}H NMR spectrum for azo compound **4** in $CDCl_3$.

The interpretation of the ^{1}H NMR spectrum shown in Figure 9, is analogue to that of azo compound **3**. The main difference is the presence of a multiplet between 1.51 and 1.26 ppm, as a consequence of the presence of a longer 11-carbon alkyl chain, which integrates 24 protons.

Therefore, the synthesis of both azo compounds was finally achieved with the required grade of purity needed for the synthesis of the LSCEs.

An additional monomer was synthetized during the development of this project in order to study its impact on the temperature range of stability of the nematic phase exhibited by the synthetized LSCEs. This feature will also influence the macroscopic response of the final material to light. In order to study this effect, an isotropic alkyloxy benzene was prepared, which does not contribute to the mesogens organization and is expected to promote a decrease of the nematic-to-isotropic phase transition temperature of the resulting elastomeric material. The reaction made to obtain undecenyloxybenzene (**5)** is shown below (Figure 10):

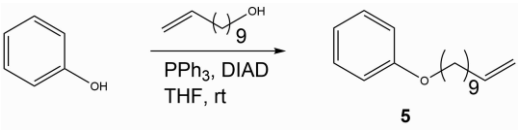

Figure 10. Synthesis of the isotropic monomer **5**

This reaction took place by means of a Mitsunobu reaction as it has been commented above. In this reaction, the alkylation of phenol was carried out, obtaining **5** in a yield of 34%.

The ^{1}H NMR recorded for compound **5** is shown in Figure 11:

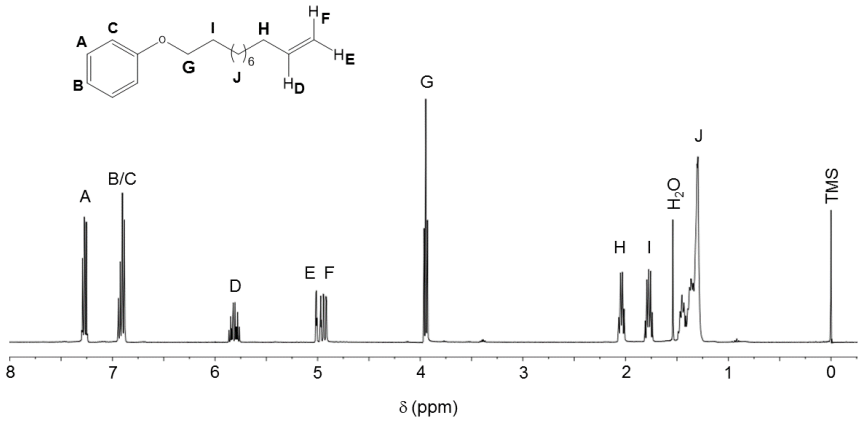

Figure 11. ^{1}H NMR spectrum for **5** in $CDCl_3$.

The alkylation process has been achieved as it can be seen in the triplet of G protons corresponding to the -O-CH_2-CH_2- segment. Also, the integration for the aromatic protons, which are 5 in total, shows up a mono-substituted benzene ring.

5.2. CHARACTERIZATION OF THE MONOMERS

5.2.1. POLARISED OPTICAL MICROSCOPY (POM)

5.2.1.1. INTRODUCTION

The anisotropy of nematic liquid crystals causes that polarised light has different velocities of propagation along the director or perpendicularly to it. This phenomenon is called birefringence. When polarized light travels through a birefringent material, the light beam is divided into two linearly polarized beams which are perpendicular to one other. One of these rays is called ordinary ray, while the second ray, is called extraordinary ray. Both rays are recombined as they exit the birefringent material. When this occurs, either a constructive or destructive interference will take place producing bright and dark regions, respectively, along the sample since there are regions with distinct orientations. Such phenomenon will produce characteristic textures for each mesophase and, therefore, will enable their identification.[13]

5.2.1.2. RESULTS

Both monomers, **3** and **4** have been studied by means of this technique in order to determine their liquid-crystalline behaviour and the temperature range where each phase is stable.

A schematic phase diagram for *trans* and *cis* isomers of the azo compound **3** is shown below:

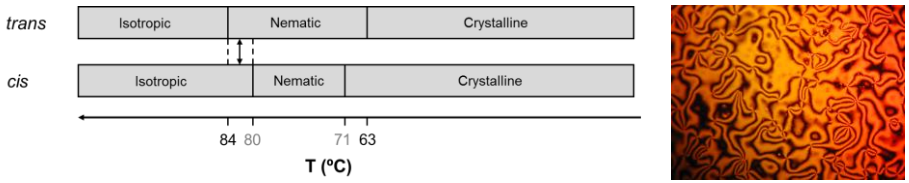

Figure 12. Schematic phase diagram obtained for both isomers of **3** in the cooling from the isotropic state (left) and photomicrograph of *trans*-**3** at 75ºC upon cooling from the isotropic liquid state (right).

Trans-**3** shows a monotropic nematic phase while cooling from the isotropic state between 84 and 63 ºC evidenced by the formation of a *schileren* texture typical of nematic phases shown

in Figure 12 (right). After irradiating *trans*-**3** with the microscope lamp in the isotropic phase, the system is isomerised to the *cis* form, which shows a smaller range of stability for the nematic phase between 80 and 71ºC. There is a small range of temperatures between 80 and 84 ºC in which can be passed from a nematic phase to an isotropic phase upon irradiating the sample (Figure 12, left). As its six-carbon alkyl chain analogue, *trans*-**4** shows a monotropic nematic phase while cooling from the isotropic phase between 90 and 73 ºC. On the other hand, *cis*-**4** shows also a nematic phase between 85 and 72 ºC. Also, there are a small range of temperatures compressed between 85 and 90 ºC in which it exists the possibility to switch between a nematic phase to an isotropic one by irradiating the sample with light (See Figure A1, appendix 1).

5.2.2. THERMAL *CIS*-TO-*TRANS* ISOMERISATION KINETICS

5.2.2.1. INTRODUCTION

The technological application of azobenzenes in novel photoactive azobenzene-based liquid-crystalline materials is closely related to the kinetics of the *cis*-to-*trans* isomerisation. Generally *trans*-to-*cis* photo-isomerisation is rapid while the thermal *cis*-to-*trans* relaxation varies greatly depending on the lateral substitution of the azobenzene chromophore.

The thermal *cis*-to-*trans* isomerisation process has been studied by means of conventional UV-Vis spectroscopy by evaluating the variation of the absorbance at λ_{max} along time under isothermal conditions. Therefore, the rate equation for the unimolecular first-order *cis*-to-*trans* isomerisation process is given by equation 2:

$$\textit{cis} \xrightarrow{k} \textit{trans}$$

$$v = -\frac{d[cis]}{dt} = k \cdot [cis] \qquad (1)$$

The integration of this differential equation in separated variables can be easily resolved, obtaining the integrated rate equation for the thermal *cis*-to-*trans* isomerisation process of the azo-dye. This equation will describe the variation of the *cis* isomer concentration with time (eq. 3).

$$\int_{[cis]_0}^{[cis]} \frac{d[cis]}{dt} = -k \int_{t_0}^{t} k \cdot dt \xrightarrow{integration} ln\frac{[cis]}{[cis]_0} = -k \cdot t \qquad (2)$$

The concentration of *cis* isomer can be expressed as a function of the absorbance by means of the Lambert-Beer's equation, obtaining equation 4:

$$ln\frac{A_\infty - A_t}{A_\infty - A_0} = -k \cdot t \xrightarrow{exponential\ form} A_t = A_\infty - (A_\infty - A_0) \cdot e^{-k \cdot t} \qquad (3)$$

Hence, the first order rate constant for the thermal *cis*-to-*trans* isomerisation process, *k*, can be obtained from the corresponding absorbance vs. time traces.

5.2.2.2. RESULTS

The experimental data obtained for the *cis*-to-*trans* isomerisation process for azo-compound **4** shown in Figure 13 confirms a first order rate constant for the isomerisation *cis*-to-*trans* process as expected. Results for **3** are analogous and are shown in table 1.

Compound	k (s^{-1})	$t_{1/2}$ (h)
3	$1.28 \cdot 10^{-3}$	9.0
4	$1.57 \cdot 10^{-3}$	7.4

Table 1. Rate constants, *k* and half-life time, $t_{1/2}$ measured at 295 K.

Those results point to a relative stability of the cis isomer enough for allowing the study of the properties of the irradiated system as it has a long half-life time. In addition, that relatively long half-life time brings the possibility to design photoactive materials with huge application under ambient conditions, due to the possibility to generate a large population of *cis* isomer that will induce to a great macroscopic deformation.

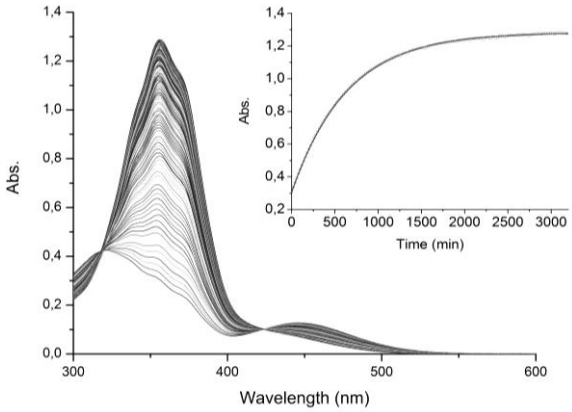

Figure 13. Changes in the electronic spectrum of a **4** *cis*-to-*trans* isomerising ethanol solution at 295 K.

5.3. SYNTHESIS OF THE LSCES

In this work, eight elastomeric samples have been prepared. A schematic representation of the composition of the LSCEs is shown below.

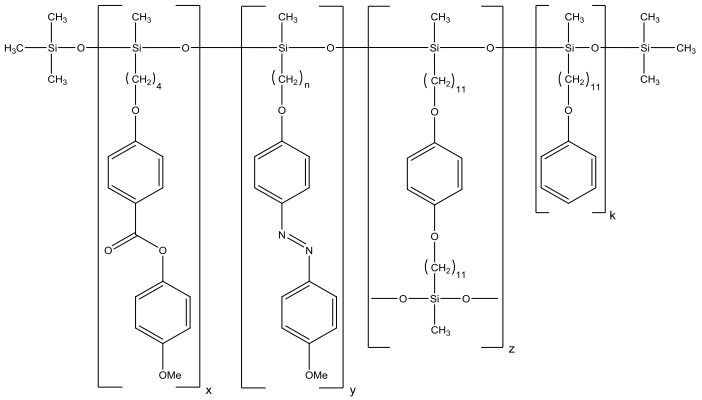

Figure 14. Chemical composition of the different LSCEs prepared.

The proportion of each monomer for the designed LSCEs is shown in Table 1.

Elastomer	x		Y	z	k
EAZO6_100	90	n = 6	-	-	-
EAZO6_75	67.5	n = 6	-	-	-
EAZO6_75_M_25	67.5	n = 6	22.5	10	-
EAZO6_60_M_40	54	n = 6	36	10	-
EAZO6_50_M_50	45	n = 6	45	10	-
EAZO11_50_M_50	45	n = 11	45	10	-
EAZO6_43_M_43_FC11_4	34.4	n = 6	34.4	10	4
EAZO6_40_M_40_FC11_10	32	n = 6	32	10	10

Table 2. Composition (%) of the synthetised LSCEs.

The preparation of the different elastomers was carried out according to the spin-casting technique in three steps developed by Küpfer and Finkelmann.[14] This technique consists in a first Pt-catalysed hydrosilylation process which takes place at 75 ºC in a centrifuge at 5000 rpm.

In this step, the different monomers, as the mesogens/s, cross-linker/s and comonomer/s react through their terminal olefin with the polysiloxane backbone. In order to achieve an elastomeric, orientable system, the reaction is stopped before is completely finished. In the second step, a uniaxial force is applied to the sample along it longest axis to obtain a monodomain elastomeric system. After the directors have been macroscopically oriented, a second cross-linking reaction is performed without removing the applied load in an oven at 75 ºC for 48 h. Finally, the LSCE is purified in order to remove both the catalyst and also unreacted monomers.

5.4. CHARACTERISATION OF THE LSCES

5.4.1. DIFFERENTIAL SCANNING CALORIMETRY (DSC)

5.4.1.1. INTRODUCTION

DSC measures the difference of heat required to keep at the same temperature a sample and a reference. The basic principle of this technique is based on the fact that when a phase transition takes place, a certain amount of heat must be provided to the sample in order to maintain the same temperature, depending on whether the transition will endothermic or exothermic. The result of a DSC experiment is a curve of heat transfer as a function of temperature called thermogram.

DSC allows not only the determination of phase transition temperatures but also the thermal range of stability of that different phases. In the present work, all the phase transition temperatures, $T_{N\text{-}I}$, and the glass transition temperatures, T_g, have been determined by means of this technique.

The value of the energetic parameters associated to these phase transitions like their enthalpy, $\Delta H_{N\text{-}I}$, can be related to the nature of the phases involved in this transition. Usually, this value is proportional to the variation of the order present in the system during the phase transformation. The value associated to the nematic-to-isotropic phase transition is in most cases between 0.5 and 5 $J \cdot g^{-1}$ whereas for the smectic-to-isotropic is between 5 to 20 $J \cdot g^{-1}$, this fact evidences that the nematic phase is less ordered than the smectic one.[15]

5.4.1.2. RESULTS

Figure 15 shows a representative DSC thermogram (see Figures in Appendix 2 for the other DSC thermograms). The corresponding thermodynamic parameters are shown in Table 2.

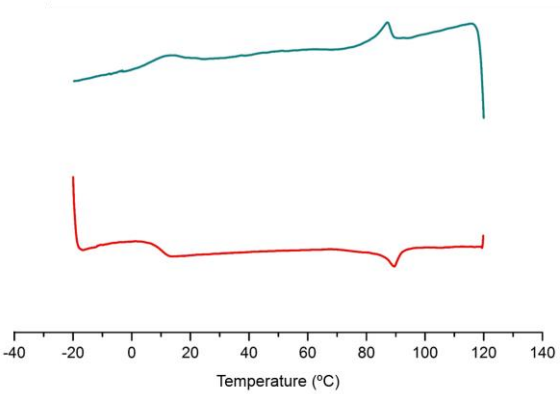

Figure 15. DSC thermogram for **EAZO6_50_M_50**. The red series stands for the heating scan, carried out at a scan rate of 10ºC/min under N_2 atmosphere and the blue series stands for the cooling one, carried out under the same conditions.

Elastomer	$T_{N\text{-}I}$ (K)	$\Delta H_{N\text{-}I}$ (J·g^{-1})
EAZO6_100	379*	1.53*
EAZO6_75	327	3.00
EAZO6_75_M_25	370	1.22
EAZO6_60_M_40	355	1.34
EAZO6_50_M_50	360	2.71
EAZO11_50_M_50	356	1.24

Table 3. Nematic-to-isotropic phase transition temperatures, $T_{N\text{-}I}$, and, nematic-to-isotropic phase transition enthalpy, $\Delta H_{N\text{-}I}$ for the synthetised elastomers. Values marked with * show a smectic mesophase.

For all the elastomers, it can be observed a phase transition with an enthalpy characteristic for the nematic-to-isotropic transition which will be posteriorly confirmed by the XRD patterns, unless for the **EAZO6_100** which shows a Smectic mesophase. Also, a broad nematic phase was manifested for both **EAZO6_75** and **EAZO6_50_M_50** between their glass transition temperatures at T_g = 292 K (ΔC_p of 0.75 J·g^{-1}·K^{-1}) and T_g = 278 K (ΔC_p of 0.14 J·g^{-1}·K^{-1}) respectively and their nematic-to-isotropic phase transition temperatures at $T_{N\text{-}I}$ = 327 K and $T_{N\text{-}I}$ = 360 K. Glass transition temperatures for the other elastomers could not be determined because the measurement set up could not reach the low temperatures needed. Except for **EAZO6_100**, nematic elastomeric systems under ambient conditions has been achieved for **EAZO6_75**, **EAZO6_75_M_25**, **EAZO6_60_M_40**, **EAZO6_50_M_50**. From the results shown in Table 3, it

can be deduced that only changing the relative proportion between that binary system (mesogen and azocompound), it is not possible to induce great variations of the T_{N-I}. To reduce the nematic-to-isotropic phase transition temperature a ternary system should be studied with the introduction of a third comonomer. It is expected that the disorder introduced in the final system by the presence of the aliphatic comonomer will induce a decrease of T_{N-I}.

5.4.2. SWELLING EXPERIMENTS

5.4.2.1. INTRODUCTION

Liquid-crystalline elastomers, cannot be dissolved in any solvent because of the presence of a cross-linking agent. The density of cross-linking units can be easily determined by the swelling experiments. These experiments are based on the fact that when a liquid-crystalline elastomer is placed into a suitable solvent, it experiments a huge deformation due to the solvent absorption.

The Flory-Rehner hypothesis considers that the free energy variation during this process is related to two additive contributions, and those are, the free energy of mixing, ΔG_{mix} and the free energy related to the elastic deformation of the system, ΔG_{el}.[16] Hence, the free energy associated to the swelling process of the elastomeric system, $\Delta G_{swelling}$, is given by equation 4.

$$\Delta G_{\text{swelling}} = \Delta G_{\text{mix}} + \Delta G_{\text{el}} \quad (4)$$

Once the system reaches the thermodynamic equilibrium, the free energy of the swelling process gets nullified, so $\Delta G_{mix} = - \Delta G_{el}$.

Swelling parameter (q) is defined as the ratio of volumes of the swollen and the initial elastomer measured under thermodynamic equilibrium conditions. Due to the anisotropy of LSCEs along their z-axis, both x- and y- dimensions will change in the same way but differently from the z- one. The swelling parameter is given by equation 5.

$$q = \frac{z \cdot x^2}{z_0 \cdot x_0^2} \quad (5)$$

For systems with similar compositions, high values of the swelling parameter can be related to low cross-linked systems and in the other way, low values of the swelling parameter can be related to high cross-linked systems.

5.4.2.2. RESULTS

The obtained values for the swelling parameter, *q*, of the synthetised elastomers are shown in Table 3.

Elastomer	Swelling parameter (*q*)
EAZO6_75	1.6
EAZO6_75_M_25	5.5
EAZO6_60_M_40	6.6
EAZO6_50_M_50	5.0
EAZO11_50_M_50	4.6

Table 4. Values of the swelling parameter for the prepared elastomers.

The results obtained for the mesogen containing elastomers are compressed between 4.6 and 6.6 showing up a similar cross-linking concentration. While for the **EAZO6_75** which does not contain the mesogenic unit, the obtained value of *q* is different matching with the observed rigidity of the elastomer due to the different mesomorphic behaviour of the sample.

5.4.3. X-RAY SCATTERING

5.4.3.1. INTRODUCTION

When X-rays hit the surface of a material, part of it is scattered by the surface atom layer. The unscrambled part penetrates the material network and is dispersed.

At any angle that fulfils the Bragg's law (Figure 16), it can be stated that the reflected rays are in phase, and therefore, they will experience constructive interferences. At any angle that does not comply Bragg's law, the rays will not be in phase, and therefore will experience destructive interference. Bragg's law is expressed by the following equation:

$$\lambda = 2d \sin\theta \qquad (6)$$

where *d* is the distance between the diffraction planes, θ is the incident angle and λ is the wavelength of the incident radiation, the used λ is 1.5418 Å which corresponds to the Cu Kα.

The diffraction pattern is the result of the superposition of spherical waves from diffraction centres. Regarding the diffraction pattern, if the sample does not show any type of order, it will not show any structure, but rather a distribution of the intensity. If the sample has a certain degree

of order, however, the diffraction pattern will show constructive interferences in certain directions, and the decrease in intensity in the others.

Nematic elastomers, either LCE or LSCEs show up a signal associated to the distance between repeated mesogenic units, usually 4-5 Å in the XRD pattern. The difference could be observed in the azimuthal intensity distribution of that signal, which is distributed throughout the entire range of angles for a LCE, while for a LSCE, is concentrated in the equatorial area.

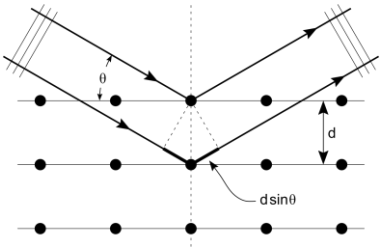

Figure 16. Schematic representation of Bragg's Law.

X-ray scattering provides some parameters which will be useful to the knowledge of the structure present in the LSCE. Firstly, in the XRD pattern, the differences between a nematic mesophase and any of the smectic ones, is pretty obvious due to the fact that in nematic LSCEs there is only one distance repeated, which is the distance between contiguous mesogens and this could be observed in the XRD pattern with a maximal intensity signal in the wide angle region (WAXS). Smectic mesophases, on the other hand, show also some signals at small angle region (SAXS) due to the distance between consecutive layers, d_l.

5.4.3.2. RESULTS

Only three of the elastomers synthetized along this project have been studied by means of this technique because of the lack of time and those are: **EAZO6_100**, **EAZO6_75** and **EAZO6_50_M_50** and the recorded diffractograms are shown in Appendix 3.

For both elastomers **EAZO6_75** and **EAZO6_50_M_50** a typical diffraction pattern for nematic structures has been observed (Figure 17, left).

Hence, the distance between the mesogenic units can be directly calculated from the data using Eq. 6 obtaining a d_m = 4.4 Å for both elastomers according to a nematic system.

On the other hand, for **EAZO6_100** diffractogram has been observed (Figure 17, right).

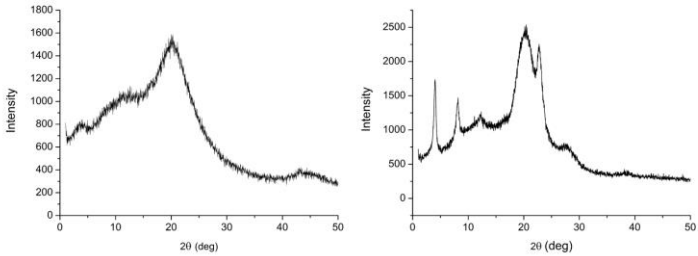

Figure 17. XRD pattern for **EAZO6_50_M_50** (right) and **EAZO6_100** (right) at room temperature.

In this case, a highly ordered layered system is observed in the presence of 3 consecutive signals in the SAXS referred to the distance between layers and also the two signals in the WAXS. From the wide angle reflex, the distance between the mesogenic units could be calculated, d_m = 4.3 Å and the distance between consecutive layers could be calculated from the small angle reflex, d_l = 10.8 Å.

To evaluate the degree of order of the prepared elastomers in order to confirm if LSCEs has been obtained correctly azimuthal intensity distribution has been measured (Figure 18).

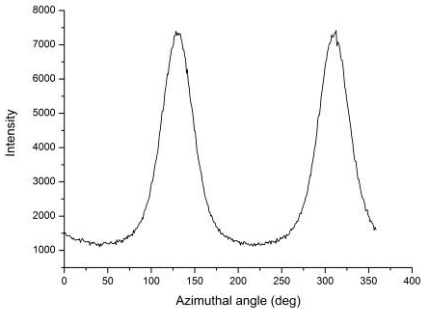

Figure 18. Azimuthal intensity distribution of **EAZO6_50_M_50** at room temperature.

As the maximum at 90º approx. has the intensity concentrated in the equatorial region of the azimuthal scan it can be confirmed that it belongs to a monodomain sample. The results for the **EAZO6_75** are analogous, so two of the three elastomers studied by XRD may exhibit a monodomain structure. In order to confirm if the obtained elastomers are monodomain or polidomain the samples will be studied by means of polarised optical microscopy (POM).

5.4.4. Polarised optical microscopy (POM)

5.4.4.1. INTRODUCTION

The main basis of this thechnique have been explained in chapter 5.2.1. More specifically for the determination of a liquid crystal structure by POM, the sample is placed between two crossed polarisers. Generally, no light passes through the second polariser because all the light emerging from the first polariser is absorbed by the second one. This changes when you enter an anisotropic material such as a liquid crystal, as long as the particles are aligned along the director axis. Therefore, when the director vector is either parallel or perpendicular to the polarisation director, the material will be shown black, as the polarisation state of the incident light doesn't change when passing through the sample. On the other hand, when the director is at any angle between 0º and 90º the sample will get some brightness because the elliptically polarised light will be parallel to the polarisation axis of the analyser twice during each cycle.

5.4.4.2. RESULTS

All the transparent or partially transparent prepared elastomers were studied by means of POM in order to determine if monodomain systems have been achieved successfully. In Figure19, photomicrographs recorded for **EAZO11_50_M_50** are shown.

Figure 19. Photomicrograph of **EAZO11_50_M_50** at 298 K.

Those images are analogous for all the prepared elastomers which contain the phenylbenzoate-based LC in their network. The samples become dark when director forms even an angle about 0 or 90º with the polarisation vector, but show brightness when it forms an angle about 45º. That can be related to monodomain samples. Both elastomers **EAZO6_100** and **EAZO6_75** could not be studied by means of POM due to their opacity.

6. EXPERIMENTAL SECTION

6.1. MATERIALS AND METHODS

6.1.1. Anhydrous solvents

CH_2Cl_2 was distilled from CaH_2; THF was distilled from sodium/benzophenone.

Thiophene-free toluene was obtained by washing commercially available toluene with concentrated sulphuric acid, dried with $CaCl_2$ and further distilled. After its purification it was stored over activated 5 Å molecular sieves.

6.1.2. Thin layer and flash column chromatography

Thin layer chromatography (TLC) was carried out using Merck silica gel 60 aluminium sheets with a fluorescent indicator (F254) and observed under UV light. Flash column chromatography was carried out over silica gel (35-70μ, Carlo Erba).

6.1.3. Nuclear Magnetic Resonance spectroscopy (NMR)

NMR spectra were collected in a Varian Mercury 400 MHz instrument. Chemical shifts are given in ppm and they have been referred to the corresponding solvent as a reference.

6.1.4. Fourier transform infrared spectroscopy (FT-IR)

ATR FT-IR spectroscopy was carried out in a FT-IR Nicolet 6700 spectrometer.

6.1.5. Analytical Weights

Precision weights were measured in a Mettler-Toledo ME204 balance (±0.1 mg).

6.1.6. UV-Vis spectroscopy

UV-Vis spectra were registered in a Varian Cary UV-Vis-NIR 500E spectrophotometer.

6.1.7. Kinetic experiments

A population of *cis*-azobenzenes was generated by UV photolysis and its relaxation was studied by time-resolved UV-Vis spectroscopy. The samples were irradiated with a Philips high-pressure mercury lamp (total nominal power 500 W) filtered with a 0.5 M solution of $Co(NO_3)_2$ in water for 10 min. Following, the solutions were thermostated in the dark at 298 K and the *cis*-to-*trans* isomerisation was monitored. Kinetic experiments were performed in 1 cm optical path quartz cells.

6.1.8. X-Ray diffraction experiments (XRD)

X-ray scattering experiments at room temperature were performed with a PANalytical X'Pert PRO MPD θ/θ powder diffractometer (radius = 240 mm) with a PIXcel detector (active length = 3.347°) in a configuration of convergent beam with a focalizing mirror and a transmission geometry. All the flat elastomeric materials were sandwiched between the low absorbing films of polyester (thickness = 3.6 μm). All the measurements were carried out with the monochromatic Cu Kα radiation (λ = 1.5418 Å) at an operating power of 45 kV (40 mA). The incident beam slits were adjusted in such a way that the beam height was equal to 400 μm. In addition, a mask defining a length of the beam over the sample in the axial direction of about 4 mm was used. 2θ/θ scans were registered from 2θ = 1° to 2θ = 60° with a step size of 2θ = 0.026°, and a measuring time of 300 s per step. On the other hand, azimuthal scans at 2θ = 20.60° and 2.81° were collected at a step size of φ = 1°, with a measuring time of 2.55 s per step.

6.1.9. Swelling experiments

Swelling experiments were performed in toluene at room temperature. The dimension of the elastomers in the deswollen and swollen state in toluene were measured with a graduated lens.

6.1.10. Polarised Optical Microscopy (POM)

Polarised optical microscopy was performed using a Nikon Eclipse polarizing microscope equipped with a Linkam THMS hot stage and a Linkam CI 93 programmable temperature controller. All measurements have been performed at a scan rate of 2 ºC·min^{-1}.

6.1.11. Differential Scanning Calorimetry (DSC)

DSC thermograms were collected in the following apparatus:

- Perkin Elmer DSC-7 apparatus under nitrogen atmosphere at 10 ºC·min^{-1}.
- Mettler-Toledo DSC821E apparatus under nitrogen atmosphere at 10 ºC·min^{-1}.

6.1.12. Spin-casting technique

In order to obtain the elastomer films, the corresponding reaction mixture was poured in a self-constructed spin-casting cell (1 cm high and 5 cm of diameter) and spin-casted using a Universal 32R Hettich centrifuge at 5000 rpm and 75 ºC. The temperature was controlled by means of a Julabo MB 5 thermostat.

6.2. SYNTHESIS OF THE MONOMERS

6.2.1. 1,4-Bis(10-undecenyloxy)benzene (1)

Hydroquinone (4.02 g, 36.5 mmol) and PPh_3 (20.1 g, 76.5 mmol) were dissolved in THF (40 cm^3) under inert atmosphere. After stirring the solution for 15 minutes at room temperature, 10-undecen-1-ol (15 cm^3, 74.9 mmol) and DIAD (15 cm^3, 76.2 mmol) were slowly added. The reaction mixture was stirred at room temperature overnight. After, the solvent was removed under reduced pressure. The crude was purified by flash column chromatography using a mixture of hexane and CH_2Cl_2 (7:3 v/v) as the eluent. The Product was recrystallized from absolute EtOH. **1** was obtained as a white solid.

Yield: 2.009 g (13%)

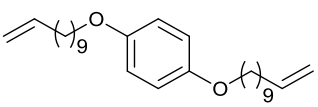

1

FT-IR: 3080 (=CH st), 2933,2918 (C_{sp3}-H st) and 1642 (C=C st) cm^{-1}. ^{1}H NMR ($CDCl_3$, 400 MHz): δ 6.81 (4H, s, H ar), 5.86-5.76 (2H, m, 2 x =CH), 5.02-4.90 (4H, m, =CH_2), 3.89 (4H, t, 2 x O-CH_2, ^3J = 6.6 Hz), 2.08-2.00 (4H, m, CH_2), 1.79-1.70 (4H, m, CH_2), 1.50-1.25 (24H, m, CH_2) ppm.

6.2.2. 4-hydroxy-4'-methoxyazobenzene (2)

4-methoxyaniline (3.04 g, 24.7 mmol) was dissolved in water (30 cm^3) and concentrated H_2SO_4 (15 cm^3). The resulting solution was cooled to 0 ºC. After, a solution of $NaNO_2$ (1.98 g, 28.7 mmol) in cold water (20 cm^3) was slowly added. The reaction mixture was stirred for 2 hours. Then, a solution of NaOH (8.20 g, 205 mmol) and phenol (2.61 g, 27.8 mmol) in water (30 cm^3) was added. The resulting solution was stirred for 1 hour. Next, a 2M HCl aqueous solution was added to the reaction mixure until pH 4-5, thereby observing the precipitation of a red solid, which

was isolated by vacuum filtration, washed thoroughly with water and dried. The solid was purified by flash column chromatography using a mixture of CH_2Cl_2 and AcOEt (4:0.5 v/v) as the eluent. **2** was obtained as a brown solid.

Yield: 4.921 g (87%)

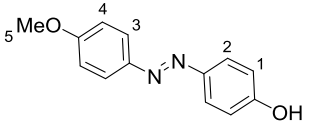

2

FT-IR (ATR): 3404 (OH st), 3026 (C_{sp2}-H st), 2985, 2950 (C_{sp3}-H st) and 1654 (C=C st) cm^{-1}. ^1H NMR ($CDCl_3$, 400 MHz): δ 7.87 (2H, d, ^3H ar, ^3J = 8.8 Hz), 7.83 (2H, d, ^2H ar, ^3J = 8.7 Hz), 7.00 (2H, d, ^4H ar, ^3J = 9.0 Hz), 6.93 (2H, d, ^1H ar, ^3J = 8.6 Hz), 5.17 (1H, s, --OH), 3.89 (3H, s, ^5H) ppm.

6.2.3. 4-(5-hexenyloxy)-4'-methoxyazobenzene (3)

2 (3.40 g, 14.9 mmol) and PPh_3 (4.63 g, 17.7 mmol) were dissolved in anhydrous THF (40 cm^3) under inert atmosphere. After stirring the solution for 15 minutes at room temperature, 5-hexen-1-ol (2.1 cm^3, 18 mmol) and DIAD (3.5 cm^3, 17.8 mmol) were added. The reaction mixture was stirred at room temperature overnight. After, the solvent was removed under reduced pressure. The crude was purified by flash column chromatography using a mixture of hexane and CH_2Cl_2 (3:2 v/v) as the eluent. **3** was obtained as a yellow solid.

Yield: 4.112 g (76%)

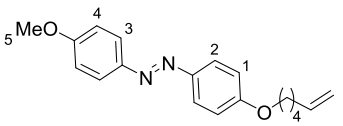

3

FT-IR (ATR): 3069 (C_{sp2}-H st), 2980, 2937, 2863, 2838 (Csp^3-H st) and 1642 (C=C st) cm^{-1}. ^1H NMR ($CDCl_3$, 400 MHz): δ 7.88 (2H, d, ^3H ar, ^3J = 8.8 Hz), 7.86 (2H, d, ^2H ar, ^3J = 8.8 Hz), 7.00 (2H, d, ^4H ar, ^3J = 8.8 Hz), 6.98 (2H, d, ^1H ar, ^3J = 8.8 Hz), 5.89-5.79 (1H, m, =CH), 5.07-5.02 (1H, m), 5.00-4.97 (1H, m), 4.04 (2H, t, ^3J = 6.5 Hz, -O-CH2-), 3.88 (3H, s, ^5H), 2.16-2.13 (2H, m, CH_2), 1.80-1.87 (2H, m, CH_2), 1.64-1.53 (2H, m, CH_2) ppm.

6.2.4. 4-(methoxy)-4'-(10-undecenyloxy)azobenzene (4)

2 (3.04 g, 13.3 mmol) and PPh_3 (3.43 g, 13.1 mmol) were dissolved in anhydrous THF (40 cm^3) under inert atmosphere and stirred overnight. After, 10-undecen-1-ol (2.6 cm^3, 12.9 mmol) and DIAD (3.0 cm^3, 15.2 mmol) were added to the resulting solution. The reaction mixture was stirred overnight. Solvent was eliminated under reduced pressure. The crude was purified by flash column chromatography using a mixure of hexane and CH_2Cl_2 (3:2 v/v) as the eluent and

recrystallized from EtOH. After, the crude was purified by flash column chromatography using a mixure of hexane and CH_2Cl_2 (8:2 v/v) as the eluent. **4** was obtained as a yellow solid.

Yield: 1.732 g (35%)

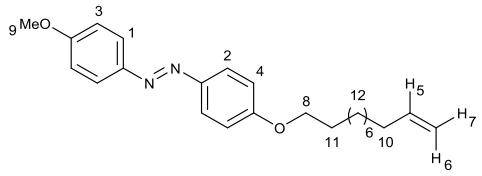

4

FT-IR (ATR): 3070 (C_{sp2}-H st), 2900, 2850 (Csp^3-H st) and 1600 (C=C st) cm^{-1}. ^{1}H NMR ($CDCl_3$, 400 MHz): δ 7.87 (2H, d, ^{1}H ar, ^3J = 8.9 Hz), 7.86 (2H, d, ^{2}H ar, ^3J = 8.9 Hz), 7.00 (2H, d, ^{3}H ar, ^3J = 7.8 Hz), 6.98 (2H, d, ^{4}H, ^3J = 7.8 Hz), 5.77-5-87 (m, 1H), 5.04-4.90 (2H, m, ^{7}H+^{6}H), 3.95 (2H, t, ^{8}H, ^3J = 6.6 Hz), 3.88 (3H, s, ^{9}H), 2.07-2.01 (2H, m, ^{10}H), 1.81-1.74 (2H, m, ^{11}H), 1.26-1.51 (m, 12H) ppm.

6.2.5. undecenyloxybenzene (5).

Phenol (3.99 g, 42.5 mmol) and PPh_3 (12.2 g, 46.5 mmol) were dissolved in anhydrous THF (20.0 cm^3) under inert atmosphere and stirred for 2 hours at room temperature. After, 10-undecen-1-ol (8.5 cm^3, 42.4 mmol) and DIAD (9.5 cm^3, 48.2 mmol) were added to the resulting solution. The reaction mixture was stirred overnight. Solvent was eliminated under reduced pressure. The crude was purified by flash column chromatography using a mixure of hexane and CH_2Cl_2 (8:2 v/v) as the eluent. **5** was obtained as a colourless oil.

Yield: 3.926 g (37%)

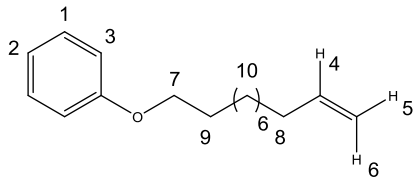

5

^{1}H NMR ($CDCl_3$, 400 MHz): δ 7.29-7.25 (2H, m, ^{1}H ar), 6.94-6.88 (3H, m, 2 x ^{3}H ar + ^{2}H ar), 5.86-5.76 (1H, m, ^{4}H), 5.02-4.96 (1H, m, ^{5}H), 4.95-4.90 (1H, m, ^{6}H), 3.95 (2H, t, ^{7}H ^3J = 6.6 Hz), 2.07-2.01 (2H, m, ^{8}H), 1.81-1.74 (2H, m, ^{9}H), 1.49-1.26 (12H, m, ^{10}H) ppm.

6.3. SYNTHESIS OF THE LIQUID SINGLE CRYSTAL ELASTOMERS

The reaction mixture was prepared by weighting the appropriate mass of each monomer (LC mesogen, azo-compound, cross-linker, alkylated phenol) and polyhydrogenomethylsyloxane (**PHMS**). This mixture was dissolved in thiophene-free toluene (1 cm^3). The reaction mixture was filtered through a Teflon filter (Millipore, 0.45 μm diameter) and the filter was washed with

tiophene-free toluene (2 x 0.5 cm^3). Then, the solution was transferred to a spinning Teflon mold, which contained a Teflon tape attached to its wall. After, a solution of $Pt(COD)Cl_2$ in anhydrous CH_2Cl_2 (30 µL) was added. The mold was properly closed and placed into the centrifuge where a first hydrosilylation reaction was carried out by spin-casting at 5000rpm at 75ºC for two hours.

Two hours later, the mold was cooled to room temperature and the elastomer was carefully removed from the tape and hung. The sample was dried for approximately 30 min at room temperature and then a uniaxial stress was applied along its long axis gradually in order to induce anisotropy in this direction.

Once the macroscopic orientation of the director was achieved, the sample was placed in the oven to fix the anisotropy achieved by means of a second hydrosilylation reaction, which took place at 75ºC for 48h. After this time, the elastomer sample was transferred to a vessel with toluene and swollen to remove the catalyst and the non-reacted monomers. Once the sample was swollen, the solvent was replaced by fresh one until the solvent remain colourless. Then, hexane was added dropwise into the vessel in order to deswell the elastomer.

Finally, the sample was removed from the vessel and hung with a small load to avoid the possible director reorientation during the drying process and introduced into the oven to dry it overnight. A table with the weights of each monomer for the synthetized elastomers is shown below.

Elastomer	Azo-compound (3)	Azo-compound (4)	L-C mesogen	Alkylated phenol (5)	C-L agent (1)
EAZO6_100	279.4	-	-	-	20.73
EAZO6_75	201.8	-	-	-	20.73
EAZO6_75_M_25	209.5	-	67.1	-	20.73
EAZO6_60_M_40	167.6	-	107.4	-	20.73
EAZO6_50_M_50	139.7	-	134.3	-	20.73
EAZO11_50_M_50	-	171.1	134.3	-	20.73
EAZO6_43_M_43_FC11_4	108.2	-	103.1	9.8	20.73
EAZO6_40_M_40_FC11_10	99.7	-	96.2	22.4	20.73

Table 5. Weight (mg) of each monomer for the synthetised LSCEs.

7. CONCLUSIONS

The main conclusions of this work are:

- All synthesis were successfully achieved and the corresponding characterisation has been done.
- The study of the photo-isomerisation process for the azobenzene derivatives synthetised was performed, obtaining a first order kinetic process with half-life times of 9.0 and 7.4 h for **3** and **4** respectively.
- Different elastomers were successfully synthetised with different composition. Also, the subsequently characterisation of the elastomeric systems was carried out by POM, DSC and XRD obtaining for all the samples nematic mesophases which are stable in a wide range of temperatures, including ambient temperature, unless for the **EAZO6_100** which presented an smectic ordering. Among that, it has been observed that $T_{N\text{-}I}$ could not be modulated in binary elastomeric systems by changing the azocompound and mesogen content. Either the variation of the azocompound content in systems with no phenyl benzoate mesogenic units had no impact on the modulation of that phase transition temperature.

In this line, a systematic study of the impact on the phase transition temperature, when introducing an aliphatic comonomer **5,** has been performed during this work in order to study the possibility to achieve good photoactuating elastomeric systems nearer ambient temperatures.

8. REFERENCES AND NOTES

1. Ware, T. H. & White, T. J. Programmed liquid crystal elastomers with tunable actuation strain. *Polym. Chem.* **6,** 4835–4844 (2015).
2. Ni, B., Xie, H. Lou, Tang, J., Zhang, H. L. & Chen, E. Q. A self-healing photoinduced-deformable material fabricated by liquid crystalline elastomers using multivalent hydrogen bonds as cross-linkers. *Chem. Commun.* **52,** 10257–10260 (2016).
3. Braun, L. B., Hessberger, T., Pütz, E., Müller, C., Giesselmann, F., A. Serra, C., Zentel, R. Actuating thermo- and photo-responsive tubes from liquid crystalline elastomers. *J. Mater. Chem. C* **6,** 9093–9101 (2018).
4. Schimpf, V., Max, J. B., Stolz, B., Heck, B. & Mülhaupt, R. Semicrystalline Non-Isocyanate Polyhydroxyurethanes as Thermoplastics and Thermoplastic Elastomers and Their Use in 3D Printing by Fused Filament Fabrication. *Macromolecules* **52,** 1, 320-331 (2018).
5. Reinitzer, F. Contributions to the knowledge of cholesterol. *Liq. Cryst.* **5,** 7–18 (1989).
6. G. W. Gray, Handbook of Liquid Crystals, Wiley-VCH, Weinheim (1998).
7. Dong, L. & Zhao, Y. Photothermally driven liquid crystal polymer actuators. *Mater. Chem. Front.* **2,** 1932–1943 (2018).
8. Otolski, C. J., Mohan Raj, A., Ramamurthy, V. & Elles, C. G. Ultrafast Dynamics of Encapsulated Molecules Reveals New Insight on the Photoisomerization Mechanism for Azobenzenes. *J. Phys. Chem. Lett.* **10**, 1, 121–127 (2018).
9. Gong, C., Yang, YH., Chen, MJ., Liu, L., Wei, Y., Tang, Q. A photoresponsive molecularly imprinted polymer with rapid visible-light-induced photoswitching for 4-ethylphenol in red wine. *Mater. Sci. Eng. C* **96,** 661–668 (2019).
10. Braun, B. L., Linder, G. T., Hessberger, T. & Zentel, R. Influence of a Crosslinker Containing an Azo Group on the Actuation Properties of a Photoactuating LCE System. *Polymers* **8,** (2016).
11. Beddoe, R. H., Sneddon, H. F. & Denton, R. M. The catalytic Mitsunobu reaction: a critical analysis of the current state-of-the-art. *Org. Biomol. Chem.* **16,** 7774–7781 (2018).
12. Heravi, M. M., Ghalavand, N., Ghanbarian, M. & Mohammadkhani, L. Applications of Mitsunobu Reaction in total synthesis of natural products. *Appl. Organomet. Chem.* **32,** e4464 (2018).
13. Chauhan, B. C. & Doshi, A. V. Mesomorphic Behavior of Chloro Substituted Azoesters. A Novel Homologous Series, 4-(4'-n-Alkoxy Benzoyloxy) Phenyl Azo-3",4"-dichlorobenzenes. *Mol. Cryst. Liq. Cryst.* **609,** 1–9 (2015).
14. Küpfer, J. & Finkelmann, H. Nematic liquid single crystal elastomers. *Die Makromol. Chemie, Rapid Commun.* **12,** 717–726 (1991).
15. He, W.-L. *et al.* Synthesis and mesophase behaviour of branched azobenzene-based supramolecular hydrogen-bonded liquid crystals. *Liq. Cryst.* **44,** 593–602 (2017).
16. The elastic free energy and the elastic equation of state: Elongation and swelling of polydimethylsiloxane networks. *J. Polym. Sci. Polym. Phys. Ed.* **13,** 683–702 (1975).

9. ABBREVIATIONS, ACRONYMS AND SYMBOLS

ATR	attenuated total reflectance
d	doublet
d_l	distance between layers
d_m	distance between monomers
DIAD	diisopropyl azodicarboxylate
DSC	differential scanning calorimetry
FT-IR	fourier transform infrared spectroscopy
hν	light promoted process
IR	infrared
J	coupling constant
k	kinetic rate constant
LC	liquid-crystal
LCE	liquid-crystal elastomer
LCP	polymeric liquid-crystal
LSCE	liquid single crystal elastomer
m	multiplet
NMR	nuclear magnetic resonance
PHMS	polyhydromethylsyloxane
POM	polarised optical microscopy
ppm	part per million
q	swelling parameter
rpm	revolutions per minute
rt	room temperature

S	order parameter
s	singlet
SAXS	small angle region
st	stretching
t	triplet
T_g	glass transition temperature
$T_{N\text{-}I}$	nematic to isotropic phase transition temperature
$t_{1/2}$	half-life time
TFG	treball de final de grau
THF	tetrahydrofuran
TLC	thin layer chromatography
UV	ultraviolet
WAXS	wide angle region
XRD	X-ray diffraction
Δ	heat-promoted process
$\Delta H_{N\text{-}I}$	nematic-to-isotropic phase transition entalphy
ΔG_{el}	elastic free energy variation
ΔG_{mix}	mixing free energy variation
$\Delta G_{swelling}$	swelling process free energy variation
δ	chemical shift
λ	wavelength
λ_{max}	maximal absorption wavelength
λ (Cu Kα)	wavelength of the x-ray incident beam Cu Kα
θ	diffraction angle
φ	azimuthal angle

APPENDICES

APPENDIX 1: SCHEMATIC PHASE DIAGRAM FOR AZO COMPOUND 4

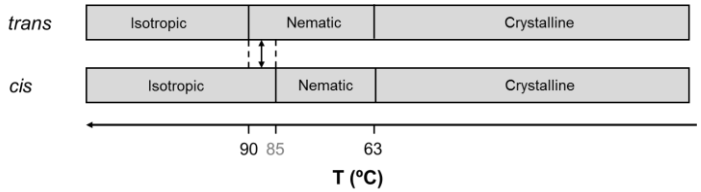

Figure A1. Schematic phase diagram obtained for both isomers of **4** in the cooling from the isotropic state.

APPENDIX 2: DSC THERMOGRAMS OF THE ELASTOMERS

- **EAZO6_100**

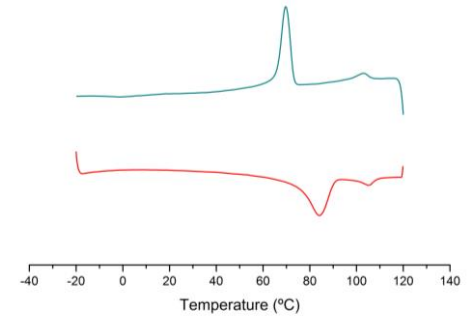

Figure B1. DSC thermogram for **EAZO6_100.** Blue series stand for the cooling from the isotropic state while the red ones stand for the heating from the crystalline state.

- **EAZO6_75_M_25**

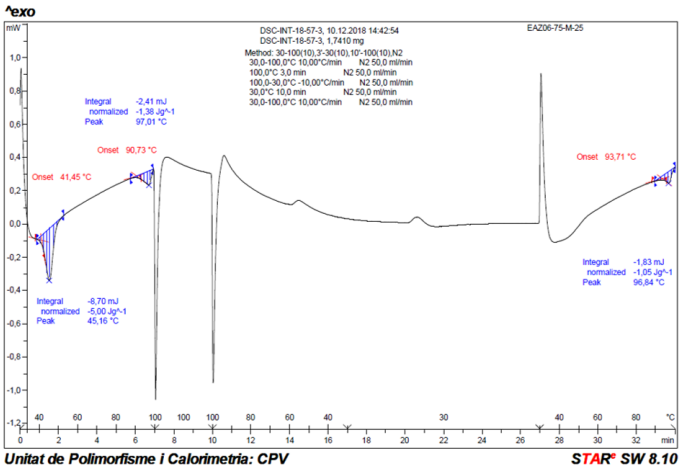

Figure B2. DSC thermogram for **EAZO6_75_M_25.** Blue series stand for the cooling from the isotropic state while the red ones stand for the heating from the crystalline state.

- **EAZO6_60_M_40**

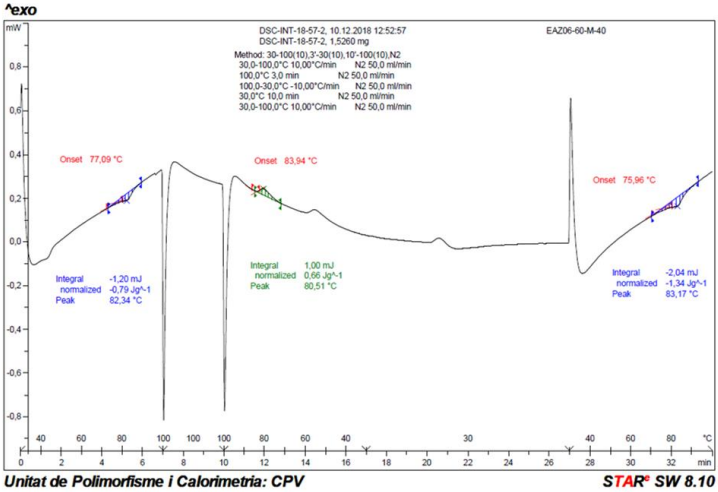

Figure B3. DSC thermogram for **EAZO6_60_M_40.** Blue series stand for the cooling from the isotropic state while the red ones stand for the heating from the crystalline state.

- **EAZO6_50_M_50**

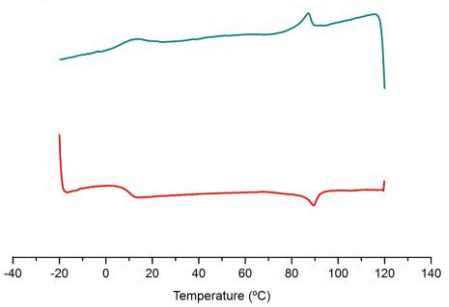

Figure B4. DSC thermogram for **EAZO6_50_M_50.** Blue series stand for the cooling from the isotropic state while the red ones stand for the heating from the crystalline state.

- **EAZO11_50_M_50**

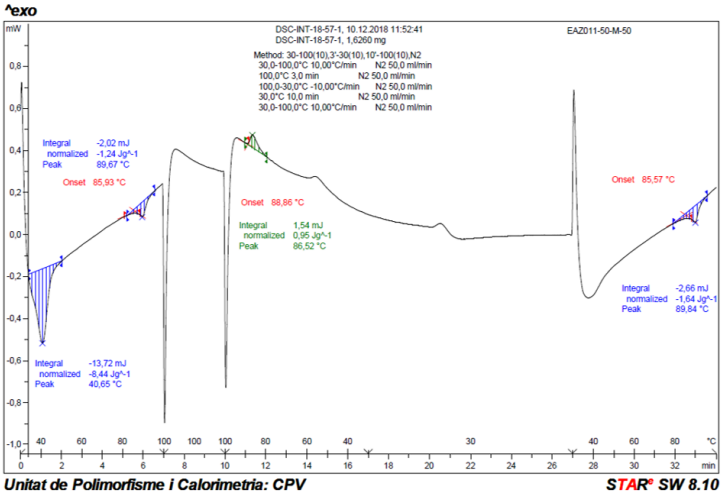

Figure B5. DSC thermogram for **EAZO11_50_M_50.** Blue series stand for the cooling from the isotropic state while the red ones stand for the heating from the crystalline state.

APPENDIX 3: XRD DIFFRACTOGRAMS FOR THE ELASTOMERS

- **EAZO6_50_M_50**

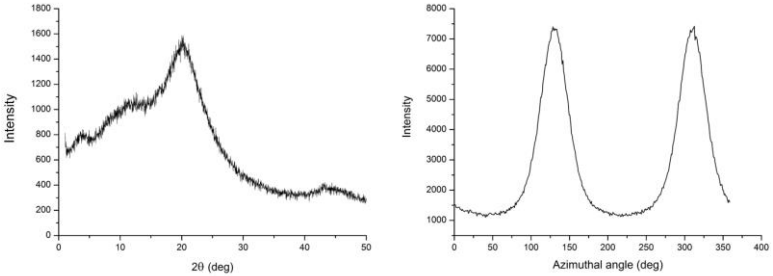

Figure C1. Radial integration of the XRD diffractogram (left) and azimuthal intensity distribution (right) of **EAZO6_50_M_50** at room temperature.

- **EAZO6_75**

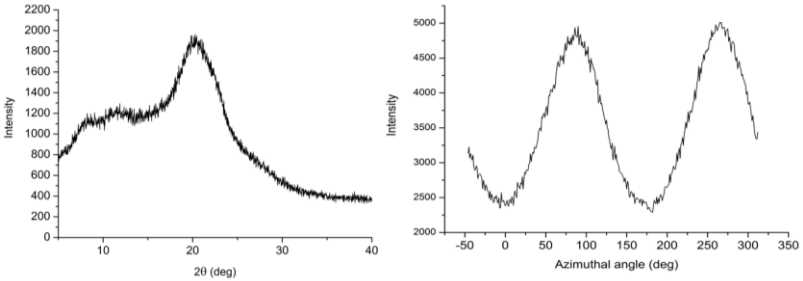

Figure C2. Radial integration of the XRD diffractogram (left) and azimuthal intensity distribution (right) of **EAZO6_75** at room temperature.

- **EAZO6_100**

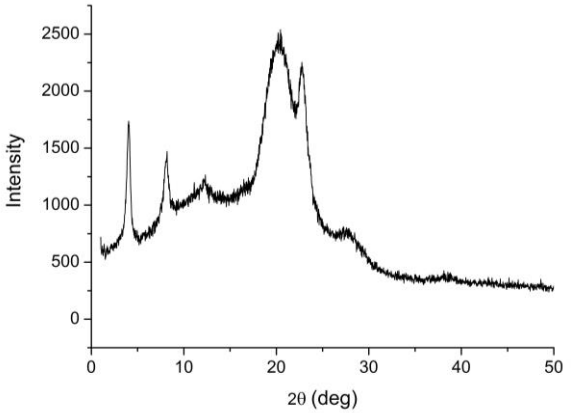

Figure C3. Radial integration of the XRD diffractogram of **EAZO6_100** at room temperature.